Optik - International Journal for Light and Electron Optics 228 (2021) 166183

Contents lists available at ScienceDirect

Optik

journal homepage: www.elsevier.com/locate/ijleo

Original research article

Propagation of Airyprime beam in uniaxial crystal orthogonal to propagation axis

Mert Bayraktar

Electric Electronic Engineering, Hasan Kalyoncu Univerity, Gaziantep, Turkey

ARTICLE INFO

Keywords:
Airyprime beam
Propagation
Uniaxial crystal

ABSTRACT

Received field expression of Airyprime beam in uniaxial crystal is derived analytically. Received field contains parabolic cylinder function which is a solution of Helmholtz euqtion in parabolic coordinates. Variations of intensity profile at the output plane is investigated considering source size, ratio of ordinary and extra-ordinary refractive indexes, and propagation length. It is seen that all selected beams take the shape of flat-topped beam. Beam having larger source size take its final shape at longer distance than smaller beams. Results of this study will be benefical for laser modulators, beam shaping, and laser applications.

1. Introduction

Recently, Airyprime beam takes place in literature [1] examinig its propagation features in free space. Truncated beam is obtained from the original case [2]. Besides this, focusing properties of circular Airyprime beam is investigated [3].

In other respects, effects of free space, atmospheric, oceanic, and biological turbulence, and uniaxial crystals on untraditional beam types are studied by scientists. Belonging to the same beam family, acceleration of airy beam along the optical axis is directly proportional to ratio of refractive indexes [4]. Similarly, intensity profiles of Airy-Gaussian beam in uniaxial crystal are plotted in [5]. It is stated [6] that autofocusing behaviour of circular Airy beam is observed when length of crystal is long enough. Effect of vortexity for Airy Gaussian vortex beams is studied in [7]. Focusing point shifts away when topological charge increases if radial polarization is applied to the same beam [8]. In addition to intensity profiles and acceleration of beam, phase structure of cosh-Airy beams is also analyzed [9]. Diffusion velocities in transverse plane become different if Airy-Hermite-Gaussian beam passes through the uniaxial cystal [10]. Received beam size for off-axis hollow vortex Gaussian beam in uniaxial crystal can be determined by controlling the refractive indexes of crystal [11]. Random electromagnetic multi-Gaussian Schell-model vortex beams turns into flat-topped beam after propagation [12]. If flat-topped beam is used on the source plane, elliptical dark hollow beam is obtained after propagation [13].

Furthermore, propagation properties of untraditional beams are also studied. Intensity profile of radially polarized Pearcey beam is shown for different conditions [14]. Self imaging property of Laguerre and Bessel beam combination is discussed in [15]. Similarly, radially polarized Laguerre-Gaussian corraleted schell model beam turns into an elliptic shape after propagation [16]. As compared to Hermite-cosine Gauss beam at the source, output beam after crystal losses its symmetry as it is stated in [17]. Flat topped beam can be obtained if higher order cosh-Gaussian beam is used in the input of the crystal [18]. It is concluded that four petal Lorentz-Gauss beam gives elliptic Gaussian-like beam after propagation [19]. Similar behavior is observed in partially cohererent case of the same beam [20].

In this study, we derived the received field of Airyprime beam propagating through uniaxial crystal. Intensity profiles are detaily

E-mail address: mert.bayraktar@hku.edu.tr.

https://doi.org/10.1016/j.ijleo.2020.166183
Received 30 July 2020; Accepted 14 December 2020
Available online 16 December 2020

analyzed depending on the changes in source beam size, ordinary and extra-ordinary refractive indexes, and propagation length.

Orientation of this article involves analytical derivation in section 2, discussion of numerical results in section 3, and concluding remarks in section 4 conclusion.

2. Analytical derivation of propagation in uniaxial crystal for Airyprime beam

We use cartesian coordinate system in this study. z-axis indicates the propagation axis and source beam is placed to $z = 0$. Transverse source plane coordinates are defined as x_0 and y_0. Received field after distance z is measured over the transverse co-ordinates x and y. Dielectric tensor of uniaxial crystal is taken as

$$\varepsilon = \begin{bmatrix} n_e^2 & 0 & 0 \\ 0 & n_0^2 & 0 \\ 0 & 0 & n_0^2 \end{bmatrix} \tag{1}$$

Where n_0 and n_e indicate ordinary and extraordinary refractive indexes of uniaxial crystal. Since there is no y polarization, source electric field expression of Airyprime beam is written as

$$\begin{bmatrix} E_x(x_0, y_0, 0) \\ E_y(x_0, y_0, 0) \end{bmatrix} = \begin{bmatrix} Ai'(\frac{x_0}{\alpha_{sx}})Ai'(-\frac{x_0}{\alpha_{sx}})Ai'(\frac{y_0}{\alpha_{sy}})Ai'(-\frac{y_0}{\alpha_{sy}}) \\ 0 \end{bmatrix} \tag{2}$$

where x_0, y_0 are the source plane coordinates and α_{sx} and α_{sy} refer to Gaussian beam widths over x and y directions respectively. Received field in uniaxial crystal is evaluated using Eq. 3 and 4 below [21]

$$E_x(x, y, z) = \exp(jkn_e z) \int_{-\infty}^{\infty}\int_{-\infty}^{\infty} \widetilde{E}_x(k_x, k_y) x\exp\left[j(k_x x + k_y y) - j\frac{k_x^2 n_e^2 + k_y^2 n_0^2}{2kn_0^2 n_e}\right] dk_x dk_y \tag{3}$$

$$E_y(x, y, z) = \exp(jkn_0 z) \int_{-\infty}^{\infty}\int_{-\infty}^{\infty} \widetilde{E}_y(k_x, k_y) x\exp\left[j(k_x x + k_y y) - j\frac{k_x^2 + k_y^2}{2kn_0}\right] dk_x dk_y \tag{4}$$

where k_x, k_y coordinates in frequency domain, n_0 and n_e are ordinary and extra-ordinary refractive indexes. Applying Fourier transform, $\widetilde{E}_a(k_x, k_y)$ can be calculated by

$$\widetilde{E}_a(k_x, k_y) = \frac{1}{(2\pi)^2}\int_{-\infty}^{\infty}\int_{-\infty}^{\infty} E_a(x_0, y_0) x\exp\left[-j(k_x x + k_y y)\right] dx_0 dy_0 \tag{5}$$

Where subscript a stands for x and y respectively. Since y component of source field is zero in our case, only x component will be taken into account. After re-organization of Eq. 3–5, received field of x component is written as

$$E_x(x,y,z) = \frac{kn_0}{2\pi jz}\exp(jkn_e z)$$
$$\int_{-\infty}^{\infty}\int_{-\infty}^{\infty} E_x(x_0,y_0) \tag{6}$$
$$\exp(\frac{jk}{2zn_e}[n_0^2(x-x_0)^2 + n_e^2(y-y_0)^2])dx_0dy_0$$

We will benefit from the relationship between the source field expression with other special functions to solve Eq. 6. For this purpose, Airyprime function can be written as

$$Ai'(x) = -\frac{x}{\pi\sqrt{3}}K_{2/3}(\frac{2}{3}x^{3/2}) \tag{7}$$

where K_v refers to imaginary argument of *vth* order modified Bessel function. Utilizing 8.407 in [22]

$$K_v(x) = \frac{j\pi}{2}\exp(\frac{jv\pi}{2})H_v^{(1)}(xe^{j\pi/2}) \tag{8}$$

where $H_v^{(1)}$ denotes *vth* order Hankel function of first kind. Similarly, application of 8.466 in [22] yields us

$$H_v^{(1)}(t) \approx \sqrt{\frac{2}{\pi t}}\exp(j(t - v\pi/2 - \pi/4)) \tag{9}$$

Combining Eqs. 7,8, and 9, Airyprime expression can be obtained as

$$Ai'(x) = -\frac{jx}{2\sqrt{3}}\sqrt{\frac{2}{\pi x}}\exp(\frac{j\pi}{3})$$
$$x\exp(j(x - \pi/3 - \pi/4)) \tag{10}$$
$$= -0.08jx^{-1/2}\sqrt{\frac{3}{j\pi}}\exp(j\pi/3)\exp(-\frac{2}{3}x^{3/2})$$

Similarly, we have

$$Ai'(x)Ai'(-x) = 6.4\text{x}10^{-5}\frac{3}{\pi}\exp(j2\pi/3)x^{-1} \tag{11}$$

Finally, received field can be evaluated via

$$E_x(x,y,z) = \frac{\left(6.4\text{x}10^{-5}\frac{3}{\pi}\exp(j2\pi/3)\right)^2 kn_0}{2\pi jz}$$
$$\exp(jkn_e z)\int_{-\infty}^{\infty}\int_{-\infty}^{\infty} x^{-1}y^{-1}dx_0dy_0 \tag{12}$$
$$\exp(\frac{jk}{2zn_e}[n_0^2(x-x_0)^2 + n_e^2(y-y_0)^2])$$

For simplicity, Eq. 12 yields

$$E_x(x,y,z) = \frac{\left(6.4\text{x}10^{-5}\frac{3}{\pi}\exp(j2\pi/3)\right)^2 kn_0}{2\pi jz} \tag{13}$$
$$x\exp(jkn_e z)U(x,z)U(y,z)$$

where

$$U(x,z) = \int_{-\infty}^{\infty} \frac{\exp(\frac{jk}{2zn_e} n_0^2 (x - x_0)^2)}{x_0} dx_0$$
$$U(y,z) = \int_{-\infty}^{\infty} \frac{\exp(\frac{jk}{2z} n_e (y - y_0)^2)}{y_0} dy_0 v \tag{14}$$

At this point, convolution property of Fourier transform is used [22]

$$U(x,z) = [f_1(\tau) \otimes f_2(\tau)] \tag{15}$$

$$U(x,z) = F^{-1}\left\{\sqrt{2}\, F_1(\xi) F_2(\xi)\right\} \tag{16}$$

Where F^{-1} refers to Fourier transform, $F_{1,2}(\xi)$ correspond to Fourier transform of $f_{1,2}(\tau)$ and convolution operation is known as

$$f_1(\tau) \otimes f_2(\tau) = \int_{-\infty}^{\infty} f_1(x_0) f_2(\tau - x_0) dx_0 \tag{17}$$

$$f_1(\tau) \otimes f_2(\tau) = \int_{-\infty}^{\infty} f_1(\xi) f_2(\xi) \exp(-j\xi\tau) d\xi \tag{18}$$

Then, Fourier transform of each sub function brings us

$$f_1(\xi) = \frac{1}{\sqrt{2}} \int_{-\infty}^{\infty} \frac{1}{\tau} \exp(j\xi\tau) d\tau = \frac{j\pi}{\sqrt{2}}$$
$$f_2(\xi) = \frac{1}{\sqrt{2}} \int_{-\infty}^{\infty} \exp(-\frac{kn_0^2}{2jzn_e}\tau^2) \exp(j\xi\tau) d\tau \tag{19}$$
$$= \sqrt{\frac{jzn_e}{kn_0^2}} \exp(-\frac{kn_0^2}{2jzn_e}\xi^2)$$

Using results of Eq. 19,$U(x,z)$ is re-organized as

$$U(x,z) = j\pi \sqrt{\frac{jzn_e}{kn_0^2}} F^{-1}\left\{\exp(-\frac{jzn_e}{2kn_0^2}\xi^2)\right\} \tag{20}$$

Inverse Fourier transform is evaluated using

$$F^{-1}\left\{\exp(-\frac{jzn_e}{2kn_0^2}\xi^2)\right\} = \frac{1}{\sqrt{2}}$$
$$x \int_{-\infty}^{\infty} \exp(-\frac{jzn_e}{2kn_0^2}\xi^2) \exp(j\xi x) d\xi \tag{21}$$

In the end, $U(x,z)$ is written as

$$U(x,z) = \frac{1}{\sqrt{2}} \sqrt{\pi} \sqrt{\frac{jzn_e}{2kn_0^2}}^{-1}$$
$$x\exp(-\frac{2kn_0^2 x^2}{8jzn_e}) D_0(\sqrt{\frac{2kn_0^2}{jzn_e}}\, \frac{x}{\sqrt{2}}) \tag{22}$$

Similarly, re-organized form of $U(y,z)$ gives us

$$U(y,z) = j\pi \sqrt{\frac{jz}{kn_e}} F^{-1}\left\{\exp(-\frac{jz}{2kn_e}\xi^2)\right\} \tag{23}$$

Applying the same approach in Eq. 21, we reach to

$$U(y,z) = \frac{1}{\sqrt{2}}\sqrt{\pi}\sqrt{\frac{jz}{2kn_e}}^{-1} \\ x\exp(-\frac{2kn_e y^2}{8jz})D_0(\sqrt{\frac{2kn_e}{jz}}\ \frac{y}{\sqrt{2}}) \tag{24}$$

As a result, received field is written as in Eq. 25

$$E_x(x,y,z) = -\frac{\left(6.4\text{x}10^{-5}\frac{3}{\pi}\exp(j2\pi/3)\right)^2 k^2 n_0^2}{2z^2} \\ x\exp(jkn_e z)\exp(-\frac{2kn_0^2 x^2}{8jzn_e})\exp(-\frac{2kn_e y^2}{8jz}) \\ xD_0(\sqrt{\frac{2kn_0^2}{jzn_e}}\ \frac{x}{\sqrt{2}})D_0(\sqrt{\frac{2kn_e}{jz}}\ \frac{y}{\sqrt{2}}) \tag{25}$$

3. Numerical results and discussions

In this section of the article, results are plotted numerically and comments on them are made. Results are plotted for the different distances $z = 1.77m$, $z = 2.97m$, and $z = 4.1m$ named as short, mid, and long distances respectively. These distances are selected according to the Rayleigh distance of the first source size setting where $\alpha_{sx} = \alpha_{sy} = 0.1mm$ case. Short, mid, and long distances are evaluating Rayleigh range with 3, 5, and 10 respectively. Moreover, variation of refractive index ratio $e = n_e/n_0$ is also taken into account.

For the short propagation distance, intensity profile of small source size symmetric Airyprime beam is shown in Fig. 1. We see that. Flatness attracts the attention on the top and the bottom of the intensity profiles. We see that beam at the output plane looks like flat-topped beam for large refractive index ratio. Output beam turns into hollowness shape in the origin when $e = 1.1$ and1.7. When small refractive index ratio is considered, intensity in the hollow reaches to zero. On the other hand, beam has higher intensity while $e = 1.7$. For the same source plane settings, all beams turn into a flat-topped shape as the propagation distance increases in Fig. 2. We see also that output beam has smaller width for the refractive index ratio selected as in the middle.

As it is seen from Fig. 3, all beams have flat-topped view. Besides this, source beam diverges more for $e = 1.7$.

Figs. 4–6 show the intensity profiles of Airyprime beam having asymmetrical source sizes as $\alpha_{sx} = 0.2mm$ and $\alpha_{sy} = 0.1mm$. As compared to the symmetric case in Fig. 1, intensity profile of output beam passing through uniaxial crystal has slight hollow when large refractive index ratio $e = 2$. For smaller ratios, normalized intensity profiles show similar distribution to each other with flat-topped shape.

When the distance is increased as shown in Fig. 5, hollow of beam propagation under condition of large e becomes deeper. In addition, other beams start to leave from each other. Beam propagating through small refractive index ration diverges less comparing with the beam propagating through $e = 1.7$.

Finally, hollowness shape turns into a flat-topped shape when propagation distance increased as in Fig. 6. Similarly, output beam from $e = 1.1$ protects its shape. In this case, output beam which is propagated through the setting where $e = 1.7$ evolves into a hollowness shape. Differently, a flat peak occurs in the bottom of the hollow.

Figs. 7–9 present normalized intensity distribution on the output plane if Airyprime beam having large source size on the source plane. At close distances, flat-topped shape starts to occur for all cases of e. Hollow at zero level is seen for small and large e values. This hollow has nearly half of the peak intensity when $e = 1.7$ as it is seen from Fig. 7.

With the increase in propagation distance as in Fig. 8, small and large e values bring us flat-topped shape. On the other hand, selected e value in the middle provides hollow in the origin.

In the end of the propagation, all beams have the same intensity profiles. They all have the same width while received beam after crystal with setting $e = 1.7$ has a slight more beam width.

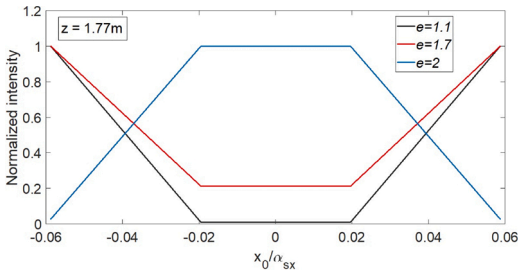

Fig. 1. Normalized intensity distribution of Airyprime beam when $\alpha_{sx} = \alpha_{sy} = 0.1mm$ and $z = 1.77m$.

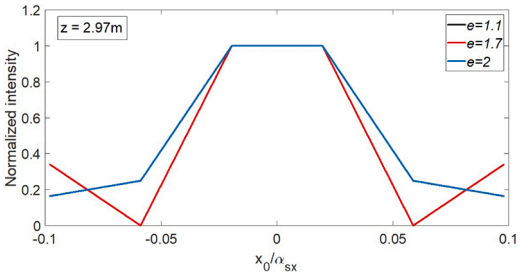

Fig. 2. Normalized intensity distribution of Airyprime beam when $\alpha_{sx} = \alpha_{sy} = 0.1mm$ and $z = 2.97m$.

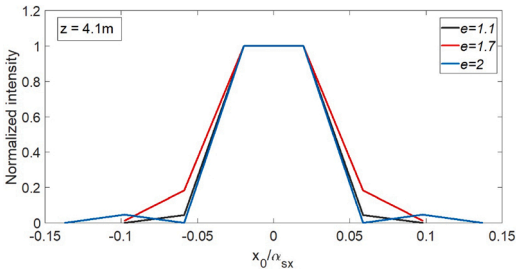

Fig. 3. Normalized intensity distribution of Airyprime beam when $\alpha_{sx} = \alpha_{sy} = 0.1mm$ and $z = 4.1m$.

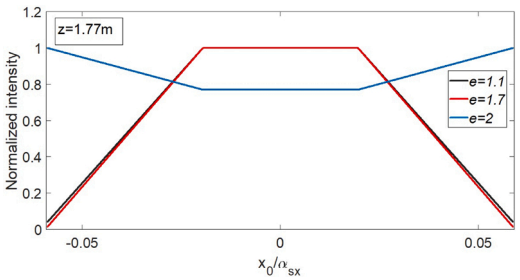

Fig. 4. Normalized intensity distribution of Airyprime beam when $\alpha_{sx} = 0.2mm$, $\alpha_{sy} = 0.1mm$ and.

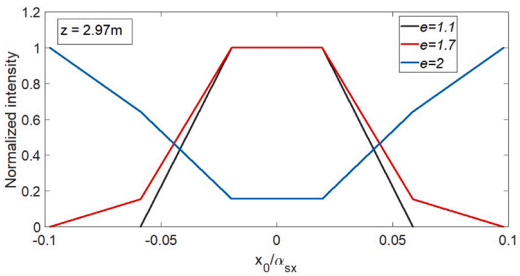

Fig. 5. Normalized intensity distribution of Airyprime beam when $\alpha_{sx} = 0.2mm$, $\alpha_{sy} = 0.1mm$ and.

4. Conclusion

Consequently, we have derived received field of Airyprime beam after propagation through uniaxial crystals. Dependence on source beam size, propagation distance, and refractive index ratios of the crystal is investigated. In the light of these, all selected beams will have a flat-topped shape after propagation. Beams having larger source size turns into final shape further comparing with smaller cases. We believe that outputs of this study will be useful for laser modulators and other laser applications.

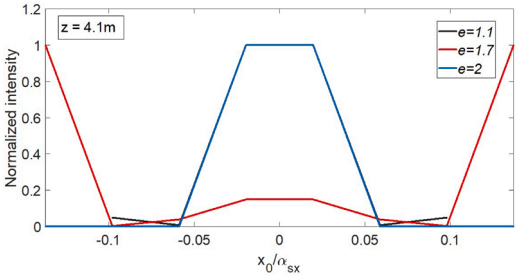

Fig. 6. Normalized intensity distribution of Airyprime beam when $\alpha_{sx} = 0.2mm$, $\alpha_{sy} = 0.1mm$ and.

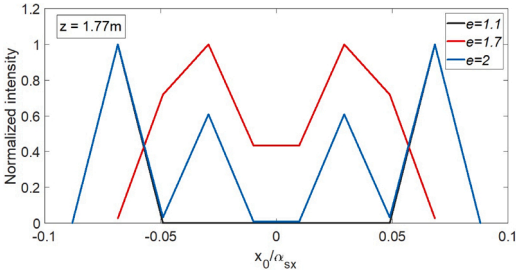

Fig. 7. Normalized intensity distribution of Airyprime beam when $\alpha_{sx} = \alpha_{sy} = 0.2mm$ and $z = 1.77m$.

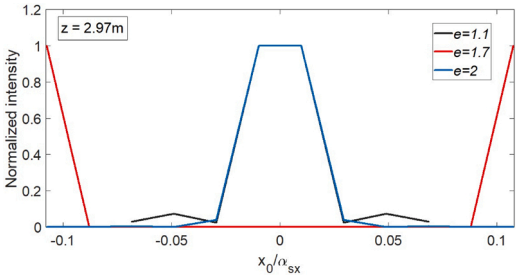

Fig. 8. Normalized intensity distribution of Airyprime beam when $\alpha_{sx} = \alpha_{sy} = 0.2mm$ and $z = 2.97m$.

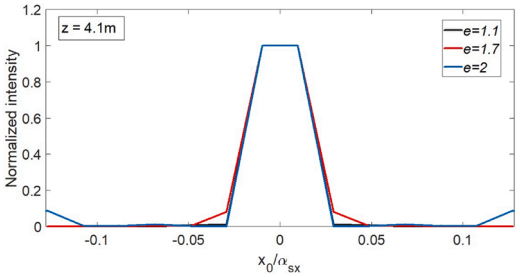

Fig. 9. Normalized intensity distribution of Airyprime beam when $\alpha_{sx} = \alpha_{sy} = 0.2mm$ and $z = 4.1m$.

Declaration of Competing Interest

The authors report no declarations of interest.

References

[1] G.Q. Zhou, R.P. Chen, G.Y. Ru, Airyprime beams and their propagation characteristics, Laser Phys. Lett. 12 (2) (2015).
[2] A. Bencheikh, Airyprime beam: From the non-truncated case to truncated one, Optik 181 (2019) 659–665.

[3] A. Bencheikh, Spatial characteristics of the truncated circular Airyprime beam, Opt. Quant. Electron. 51 (1) (2019).
[4] G.Q. Zhou, R.P. Chen, X.X. Chu, Propagation of Airy beams in uniaxial crystals orthogonal to the optical axis, Opt. Express 20 (3) (2012) 2196–2205.
[5] M.L. Zhou, C.D. Chen, B. Chen, X. Peng, Y.L. Peng, D.M. Deng, Propagation of an Airy-Gaussian beam in uniaxial crystals, Chin. Phys. B 24 (12) (2015).
[6] G.L. Zheng, X.Q. Deng, S.X. Xu, Q.Y. Wu, Propagation dynamics of a circular Airy beam in a uniaxial crystal, Appl. Opt. 56 (9) (2017) 2444–2448.
[7] W.H. Yu, R.H. Zhao, F. Deng, J.Y. Huang, C.D. Chen, X.B. Yang, Y.P. Zhao, D.M. Deng, Propagation of Airy Gaussian vortex beams in uniaxial crystals, Chin. Phys. B 25 (4) (2016).
[8] Q. Yang, W.Z. Zhu, C.J. Xu, M.Y. Lu, X.P. Chen, D.M. Deng, L.Q. Huang, Propagation of the radially polarized Airy vortex beams in uniaxial crystals orthogonal to the optical axis, J. Opt. Soc. Am. A 36 (6) (2019) 994–1002.
[9] G.Q. Zhou, R.P. Chen, X.X. Chu, Propagation of cosh-Airy beams in uniaxial crystals orthogonal to the optical axis, Opt. Laser Technol. 116 (2019) 72–82.
[10] J. Yu, S.L. Xiao, L. Yao, S.Y. Liu, J. Li, Propagation of the finite energy Airy-Hermite-Gaussian beams in uniaxial crystals orthogonal to the optical axis, J. Mod. Opt. 64 (6) (2017) 616–623.
[11] L. Li, Y.Z. Huan, Y.C. Wang, D. Hua, X. Yang, D.J. Liu, Y.X. Wang, The effects of uniaxial crystal on off-axis hollow vortex Gaussian beams, Optik 194 (2019).
[12] X.L. Ma, G.Q. Wang, H.Y. Zhong, A.Y. Dong, Y.C. Wang, D.J. Liu, Evolutions of random electromagnetic multi-Gaussian Schell-model vortex beams propagating in uniaxial crystals orthogonal to the optical axis, Optik 203 (2020).
[13] D.J. Liu, Y.C. Wang, G.Q. Wang, H.M. Yin, Propagation properties of flat-topped vortex hollow beam in uniaxial crystals orthogonal to the optical axis, Optik 127 (19) (2016) 7842–7851.
[14] C.J. Xu, L.D. Lin, Z.Z. Huang, Y.Z. Chen, X.B. Yang, H.Z. Liu, D.M. Deng, Propagation of a radially polarized Pearcey beam in uniaxial crystals, Laser Phys. 28 (11) (2018).
[15] G. Cincotti, A. Ciattoni, C. Palma, Laguerre-Gauss and Bessel-Gauss beams in uniaxial crystals, J. Opt. Soc. Am. A 19 (8) (2002) 1680–1688.
[16] J.B. Su, C.A. Xu, H.F. Xu, J. Qu, Evolution properties of the radially polarized Laguerre-Gaussian-correlated Schell-model beams propagating in uniaxial crystals, J. Opt. Soc. Am. A 37 (4) (2020) 529–539.
[17] B. Tang, Hermite-cosine-Gaussian beams propagating in uniaxial crystals orthogonal to the optical axis, J. Opt. Soc. Am. A 26 (12) (2009) 2480–2487.
[18] J. Li, Y. Chen, Y. Xin, S. Xu, Propagation of higher-order cosh-Gaussian beams in uniaxial crystals orthogonal to the optical axis, Eur. Phys. J. D 57 (3) (2010) 419–425.
[19] D.J. Liu, G.Q. Wang, H.Y. Zhong, H.M. Yin, A.Y. Dong, Y.C. Wang, Properties of a four-petal Lorentz-Gauss beam propagating in uniaxial crystal orthogonal to the optical axis, Optik 183 (2019) 257–265.
[20] D.J. Liu, H.Y. Zhong, G.Q. Wang, H.M. Yin, Y.C. Wang, Evolution properties of a partially coherent Lorentz-Gauss vortex beam in a uniaxial crystal, J. Mod. Opt. 66 (1) (2019) 67–76.
[21] A. Ciattoni, C. Palma, Optical propagation in uniaxial crystals orthogonal to the optical axis: paraxial theory and beyond, J. Opt. Soc. Am. A 20 (11) (2003) 2163–2171.
[22] I.S. Gradshteyn, I.M. Ryzhik, Table of Integrals, Series, and Products, Academic Press, 2015.